Biochemical and Biophysical Research Communications 388 (2009) 107–111

Contents lists available at ScienceDirect

Biochemical and Biophysical Research Communications

journal homepage: www.elsevier.com/locate/ybbrc

The quaternary structure of *Escherichia coli N*-acetylneuraminate lyase is essential for functional expression

Sean R.A. Devenish *, Juliet A. Gerrard *

School of Biological Sciences, University of Canterbury, Christchurch, New Zealand

ARTICLE INFO

Article history:
Received 15 July 2009
Available online 30 July 2009

Keywords:
N-acetylneuraminate lyase
Quaternary structure
Enzyme kinetics
Protein stability
Functional expression

ABSTRACT

As part of a general study into the impact of quaternary structure on enzyme function, a library of 31 point mutations were engineered at the dimer–dimer interface of the homotetrameric $(\beta/\alpha)_8$-barrel protein, *N*-acetylneuraminate lyase (NAL, EC 4.1.3.3). Disruption of the interface generated either soluble tetramers or putative dimers that were absolutely insoluble and inactive. Intriguingly, the soluble tetramers were found to have widely varying k_{cat} values, hinting at a role for the interface in catalysis. Leucine 171 was identified as essential to interface integrity. We conclude that the dimer–dimer interface of NAL is intolerant to mutation and essential for functional expression.

Introduction

The quaternary structure of proteins has piqued recent interest in the literature as a potential modulator of protein dynamics [1–5], which are increasingly recognised as being critical for enzyme catalysis [6]. We have been engaged in a comprehensive study of how quaternary structure impacts on enzyme function, using a $(\beta/\alpha)_8$-barrel protein, dihydrodipicolinate synthase (DHDPS, EC 4.2.1.52) as a model [3,4,7]. This study supports the hypothesis that quaternary structure plays a role in structure–function relationships in this family by fine-tuning the dynamics of the system for optimal catalysis [5]. Here, we extend this work to a related $(\beta/\alpha)_8$-barrel protein: *N*-acetylneuraminate lyase (NAL, EC 4.1.3.3).

NAL is a $(\beta/\alpha)_8$-barrel protein belonging to the dihydrodipicolinate synthase (DHDPS, EC 4.2.1.52) family of enzymes [8]. Like the much more closely studied DHDPS, NAL is a homotetrameric enzyme, with the monomers arranged as a dimer of tight dimers. As in DHDPS, the active site is located inside the barrel, centred about the critical catalytic residue, lysine 165, which forms a Schiff base with the first substrate, pyruvate, to facilitate the required aldol chemistry. However, the substrates and products are very different for the two enzymes, making NAL an ideal test of our hypothesis that the role played by quaternary structure in DHDPS can be generalised to other proteins.

Although closely structurally related to DHDPS, NAL plays an unconnected metabolic role, catalysing the ultimate step in sialic acid biosynthesis—the condensation of pyruvate and *N*-acetylmannosamine. The sialic acids are a large family of sugars derived from the parent compound *N*-acetylneuraminic acid [9], widely utilised on the surface of cells in animals, where they play important roles in a variety of critical biological processes, including cellular recognition and adhesion [10]. Sialic acids are less commonly found amongst bacteria, but occur on the surface of a number of pathogenic bacteria, where they are thought to provide camouflage from the host immune system [11] or to facilitate tissue invasion [12]. Bacteria may be dependent on their host for sialic acid supply or, as is the case for *Escherichia coli*, produce sialic acid themselves [11]. NAL has also found utility in the industrial synthesis of *N*-acetylneuraminic acid and related compounds [13] and attracted interest as a drug target [11,14].

To examine whether the critical nature of the dimer–dimer interface in DHDPS extended to the related enzyme NAL, we produced a library of point mutants of key residues in this interface and examined the catalytic and biophysical properties of the mutants.

Materials and methods

Materials. Unless otherwise stated, all chemicals were obtained from Sigma Chemical Company (St. Louis, MO, USA) or Codexis Inc. (Redwood City, CA, USA). Protein concentration was measured on a NanoDrop ND-1000 spectrophotometer (Wilmington, DE, USA) at 280 nm, with absorption coefficients calculated using the Protein Calculator v 3.3 (http://www.scripps.edu/~cdputnam/protcalc.html).

Abbreviations: NAL, *N*-acetylneuraminate lyase; DHDPS, dihydrodipicolinate synthase.

* Corresponding authors.
E-mail addresses: sean.devenish@canterbury.ac.nz (S.R.A. Devenish), juliet.gerrard@canterbury.ac.nz (J.A. Gerrard).

0006-291X/$ - see front matter © 2009 Elsevier Inc. All rights reserved.
doi:10.1016/j.bbrc.2009.07.128

Enzymes were manipulated at 4 °C, or on ice, and were stored in Tris–HCl buffer (20 mM, pH 8) at −80 °C.

Cloning and mutagenesis. The gene *nan*A which codes for NAL was cloned from *E. coli* W3110 genomic DNA using PCR with the primers nanAfwd: 5′-TATAGGTCTCACATGGCAACGAATTTACGTG-3′ and nanArev: 5′-TCACTCGAGTTATCACCCGCGCTCTTG-3′. The PCR product was ligated into the pGEM®-T (Promega Corporation, Madison, WI, USA) vector, and used to transform chemically competent XL-1 Blue cells (Stratagene, La Jolla, CA, USA). Plasmid was purified from isolated colonies and sequenced to confirm the correct insertion of the *nan*A gene. The *nan*A gene was then excised using the enzymes BsaI and XhoI, with the ~1 kb band purified by gel electrophoresis. Simultaneously, the vector pETM-11 [15] was cut with XhoI and NcoI to generate compatible ends, and the ~5 kb fragment purified by gel electrophoresis. These purified fragments were then ligated using T4 ligase (Invitrogen, Carlsbad, CA, USA) to give plasmid pSD03, which was used to transform chemically competent XL-1 Blue cells (Stratagene). Again, plasmid was purified from isolated colonies and sequenced to confirm the sequence of pSD03.

Site-directed mutagenesis was carried out using a QuikChange Site Directed Mutagenesis Kit (Stratagene) according to the manufacturer's instructions. The template used was pSD03, or derivatives thereof in the case of double and triple mutants. The primers used for mutagenesis are shown below in Table 1. The presence of the expected mutation was confirmed in all cases by sequencing (Canterbury Sequencing, New Zealand) plasmid extracted from isolated clones.

Over-expression and purification. Proteins were over-expressed using the auto-induction system developed by Studier [16]. Briefly, overnight LB cultures of BL21 Star (DE3) carrying the plasmid pSD03 or a mutant derivative thereof were used to inoculate 800 mL of ZYM-5052 auto-induction broth. Growth was initiated at 37 °C for about 4 h, and cultures were then shaken at room temperature overnight to allow protein expression. Cells were harvested by centrifugation (12,000 rpm, 4 °C, 10 min) and resuspended in Buffer A (20 mM sodium phosphate pH 8.0, 500 mM NaCl) containing 50 mM imidazole. Cell lysis was effected by ultrasonication on ice (2 min, pulsed 1 s on and 5 s off; Vibra-Cell VC750, Sonics & Materials, Inc., Newtown, CT, USA), and the crude cell lysate was clarified by centrifugation (15,000 rpm, 4 °C, 20 min) before loading on a 5 mL HisTrap™ FF Crude column (GE Life Sciences, Uppsala, Sweden). The column was washed with buffer A containing 30 mM imidazole until no more protein eluted (as determined using Bio-Rad Protein Dye) before elution of the bound NAL with buffer A containing 300 mM imidazole. Protein containing fractions were combined and exchanged into 20 mM Tris–HCl pH 8.0 using a desalting column (GE Life Sciences). His-tag cleavage was carried out using TEV protease prepared in-house following the method of Waugh et al. [17]. The His-tag cleaved protein was separated from TEV protease, free His-tag and uncleaved NAL by repassage through a 5 mL HisTrap™ FF Crude column before buffer exchange into 20 mM sodium phosphate pH 8.0 for storage at −80 °C.

Size exclusion chromatography. Purified NAL and mutants were run on a Superdex 200 10/300 GL column (GE Life Sciences) that had been equilibrated to 20 mM sodium phosphate pH 8.0, eluting with the same buffer. The column was calibrated using bovine serum albumin, with monomer and dimer peaks of 66 and 132 kDa, and the retention times of soluble mutant proteins were compared to that of wild-type NAL to confirm quaternary structure.

Thermal stability measurements. The melting temperature of wild-type NAL and that of soluble mutants were determined by differential scanning fluorimetry using a minor variation on the method of Nordlund et al. [18]. Briefly, the protein samples (4 μL) were added with mixing to buffer (20 μL) and SYPRO orange dye (1 μL, diluted 20-fold from supplied concentration with dH_2O) in a 96-well microplate. After sealing the plate, a stepped thermal melt program starting at 20 °C and finishing at 95 °C increasing in 0.3 °C increments, with a dwell time of 20 s after each temperature rise, was run on a Bio-Rad iCycler iQ5 Multicolour Real-Time PCR Detection System. Fluorescence measurements were obtained at the end of each dwell time. The reading of a blank well containing buffer and dye but lacking protein was subtracted from each sample reading. Melting temperatures were calculated as the temperature of maximum inflection of the melting curve. Triplicate samples were measured.

Kinetics. The catalytic activity of NAL was measured for the reverse reaction, using a coupled assay with lactate dehydrogenase, as previously described [19], with the following modifications. Assays were performed in sodium phosphate buffer (100 mM, pH 7.6) at 30 °C, kept constant using a circulating water bath. Care was taken to ensure that the enzymes and substrates were stable over the course of the assay (usually 2 min) and to ensure an excess of lactate dehydrogenase; about 100 μg per assay was used. The amount of enzyme added to each assay depended on the activity of the individual mutants, ensuring that enzyme concentration was proportional to initial rate. Initial velocities were measured in at least duplicate and were usually reproducible within 10% error.

Initial rate data were analysed using the programme OriginPro 8 (OriginLab Corporation, Northampton, MA, USA) and were fitted to the Michaelis–Menten kinetic model (Eq. (1)):

$$v = VA/(K_M + A) \quad (1)$$

Here V is the maximal velocity, A is the substrate concentration, K_M the apparent Michaelis–Menten constant, and v is the initial velocity [20].

Circular dichroism (CD) spectroscopy. CD spectra were measured using a Jasco J-815 circular dichroism spectrophotometer. Spectra were collected at a final enzyme concentration of 0.176 mg/mL in

Table 1
Primers used for site-directed mutagenesis. Mutated codons are underlined, with the particular mutated bases shown in lower case. All primers are presented in the 5′–3′ orientation.

Mutation	Forward primer	Reverse primer
L171D	GACCTCTGGCGATgaCTATCAGATGGAGCAGATCCG	CGGATCTGCTCCATCTGATAGtcATCGCCAGAGGTC
L171N	CAGACCTCTGGCGATaaCTATCAGATGGAGCAGATCC	GGATCTGCTCCATCTGATAGttATCGCCAGAGGTCTG
L171R	GACCTCTGGCGATCgCTATCAGATGGAGC	GCTCCATCTGATAGcGATCGCCAGAGGTC
L199D	CGCCTCTGGTCTGgacGCGGGCGCTGATGGTGG	CCACCATCAGCGCCCCGCgtcCAGACCAGAGGCG
L199N	CGCCTCTGGTCTGaacGCGGGCGCTGATGGTG	CACCATCAGCGCCCGCgttCAGACCAGAGGCG
L199R	CCTCTGGTCTGCgGCGGGCGCTG	CAGCGCCCGCCcGCAGACCAGAGG
I229D	GCGCTGAAAGAAGGCGATgaCCAGACCGCGC	GCGCGGTCTGGtcATCGCCTTCTTTCAGCGC
I229N	GCTGAAAGAAGGCGATAaCCAGACCGCGC	GCGCGGTCTGGtTATCGCCTTCTTTCAGC
I229R	CGCTGAAAGAAGGCGATcgCCAGACCGCGC	GCGCGGTCTGGcgATCGCCTTCTTTCAGCG

sodium phosphate buffer (20 mM, pH 8.0). Wavelength scans were collected at 20 °C using a 0.2 cm path-length cuvette, 1.0 mm bandwidth, 0.5 nm step size, and a 1 s averaging time.

Results and discussion

Interface analysis

Fig. 1 shows the X-ray crystal structure of NAL (PDB ID 1NAL, [21]) highlighting the residues of the dimer–dimer interface. As for DHDPS, the interdimeric interface is significantly weaker than the intradimeric, with 992 and 1143 Å of surface area buried, respectively (8.1% and 9.3% of total surface area, determined using PISA [22]), although the difference between the interfaces is less pronounced than observed for DHDPS. In the case of *E. coli* DHDPS, the interfaces represent 4.3% and 11.2% of the total surface area, respectively, and the weaker interface was successfully disrupted by both of the single mutations L197Y and L197D [4]. Similarly, a dimer of *M. tuberculosis* DHDPS (Evans et al., unpublished) has recently been successfully generated in our laboratory, with an interdimeric interface of 869 Å of surface area buried (7.4% of total surface area). Thus we were optimistic that a dimeric NAL could be simply generated *via* point mutation.

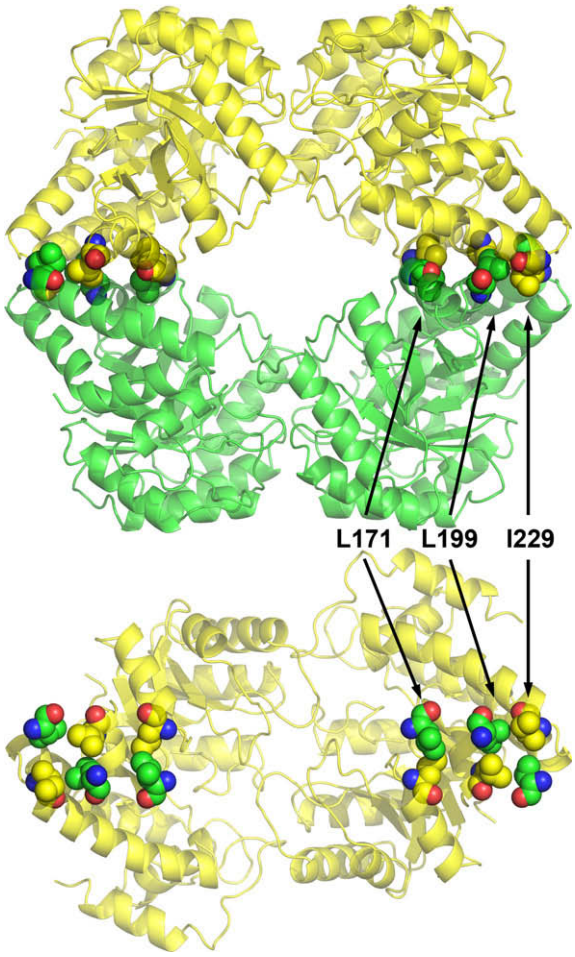

Fig. 1. NAL structure highlighting the residues selected for mutation. Tight dimer units are shown in yellow and green. Structure is viewed from the side (top) and from the bottom with one tight dimer removed (bottom). (For interpretation of the references to colour in this figure legend, the reader is referred to the web version of this article.)

Inspection of the interface (Figs. 1 and 2) and precedent from the DHDPS enzyme, suggested that hydrophobic, well-buried residues that interacted with their counterpart on the opposing monomer were ideal to maximise the effect of any changes. PISA [22] and JavaProtein Dossier [23] webservers highlighted L171, L199 and I229 as residues worth targeting for mutation (Fig. 1). It was decided to mutate each of these hydrophobic residues into a negatively charged (aspartate), positively charged (arginine) and polar uncharged (asparagine) derivative, to maximise the chances of obtaining soluble dimeric protein.

Single mutants

The full suite of nine mutant proteins was generated by site-directed mutagenesis. Soluble protein was isolated from only one of the L171 and L199 mutants, but all three of the I229 mutants were found to be soluble. The kinetic behaviour of all of the soluble mutants was examined (Table 2, Supplementary Fig. S1), with the mutated proteins showing some variation in kinetic parameters. The k_{cat} varied between 4.69 ± 0.05 and 7.72 ± 0.05 s^{-1}, while the apparent K_M for the substrate *N*-acetylneuraminic acid varied between 3.42 ± 0.08 and 5.01 ± 0.17 mM, values which are comparable to the wild-type enzyme with a K_M of 4.1 ± 0.2 mM and k_{cat} of 6.75 ± 0.08 s^{-1}.

The oligomeric structure of each soluble NAL protein was examined by gel filtration chromatography, with the wild-type enzyme and all of the soluble mutants eluting as tetramers at the same volume. To determine whether there was any change in overall stability, thermal stabilities of the wild-type and mutant NAL enzymes were investigated by differential scanning fluorimetry (DSF) [18], with all of the mutants showing lower thermal stability than the wild-type enzyme (Table 2), suggesting that the dimer–dimer interface was destabilised.

In all cases of insoluble mutants, over-expression of the mutant protein was confirmed by SDS–PAGE, in which a strong band of ~35 kDa, corresponding to the expected mass of the His-tagged NAL monomer, was seen in both the whole cell and insoluble cell debris fractions, but was entirely absent from the crude soluble extract and the eluent from a His-Trap column (Supplementary Information, Fig. S2). Considerable efforts were made to refold the insoluble mutant L199D. The cell debris was solubilised using 6 M guanidine hydrochloride and purified by His-Trap chromatography, including 6 M guanidine hydrochloride in all buffers. The purified protein was then rapidly diluted into buffer containing a variety of additives, including salt, detergents, sucrose, arginine, PEG and the substrates pyruvate and *N*-acetylneuraminic acid. In no case could activity above background oxidation of NADH be detected after the attempted refolding. The aggregated insoluble proteins did not show fluoresence with ThT, ruling out the possibility that the precipitate was amyloid-like (data not shown). We hypothesise that L171 is key to the interface and that the insolubility of these mutants was caused by successful disruption of the tetramer, but that dimer formation was accompanied by concomitant nonspecific aggregation. In order to create soluble dimeric species, we examined combinations of double and triple mutants.

Double and triple mutants

Twenty-three double mutants were generated, of which the vast majority were insoluble; however, active soluble enzyme was isolated in five cases (Table 3). Two of these proteins (L171N-I229N and L199N-I229D) co-purified from the His-column with contaminating proteins which could not be removed by further chromatography (modification or repetition of the affinity column procedure and ion exchange chromatography were attempted). The k_{cat} values for the double mutants varied signifi-

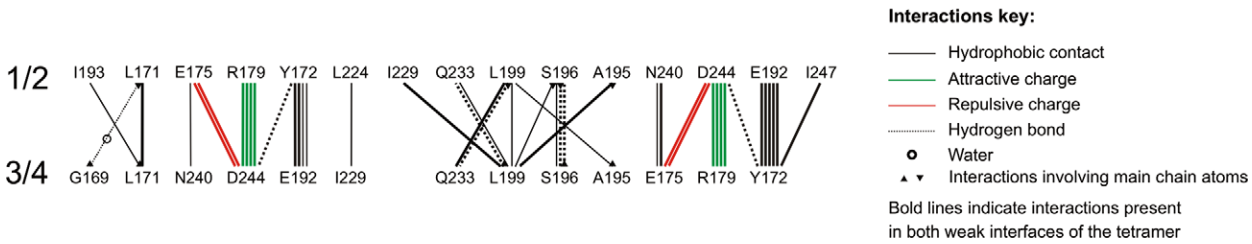

Fig. 2. Diagram of interactions across the weak interface of NAL identified by visual inspection and using JavaProtein Dossier [23].

Table 2
Kinetic parameters, thermal stability and quaternary state of NAL single mutants.

	K_M (mM)	k_{cat} (s^{-1})	T_m (°C)	Quaternary state
Wild-type	4.1 ± 0.2	6.75 ± 0.08	84.0	Tetramer
Leu171Asp		Insoluble		
Leu171Asn		Insoluble		
Leu171Arg	3.42 ± 0.08	5.49 ± 0.03	67.6	Tetramer
Leu199Asp		Insoluble		
Leu199Asn	4.3 ± 0.2	7.94 ± 0.08	52.6	Tetramer
Leu199Arg		Insoluble		
Ile229Asp	5.0 ± 0.2	4.69 ± 0.05	82.4	Tetramer
Ile229Asn	3.4 ± 0.2	7.4 ± 0.1	46.5	Tetramer
Ile229Arg	3.93 ± 0.08	7.72 ± 0.05	59.7	Tetramer

Table 3
Insoluble double mutants, and kinetic parameters, thermal stability and quaternary state of soluble NAL double mutants.

Insoluble double mutants		
Leu171Asp, Leu199Asn	Leu171Asn, Leu199Asp	Leu171Arg, Leu199Asn
Leu171Asp, Leu199Asp	Leu171Asn, Leu199Asn	Leu171Arg, Leu199Arg
Leu171Asp, Ile229Asp	Leu171Asn, Leu199Arg	Leu171Arg, Ile229Asp
Leu171Asp, Ile229Asn	Leu171Asn, Ile229Asp	Leu171Arg, Ile229Asn
Leu171Asp, Ile229Arg	Leu171Asn, Ile229Arg	Leu171Arg, Ile229Arg
Leu199Asp, Ile229Asp	Leu199Asp, Ile229Asn	Leu199Arg, Ile229Arg

	K_M (mM)	k_{cat} (s^{-1})	T_m (°C)	Quaternary state
Soluble double mutants				
Leu199Asn, Ile229Arg	4.0 ± 0.4	8.9 ± 0.2	36.8	Tetramer
Leu199Arg, Ile229Asn	6.1 ± 0.1	11.87 ± 0.06	46.1	Tetramer
Leu199Asn, Ile229Asn	4.7 ± 0.2	0.664 ± 0.009	43.9	Tetramer
Leu171Asn, Ile229Asn	2.51 ± 0.09	3.15 ± 0.03	—[a]	Impure tetramer
Leu199Asn, Ile229Asp	3.2 ± 0.4	0.29 ± 0.01	—[a]	Impure tetramer

[a] These proteins did not give interpretable melting curves by DSF, likely due to the presence of associated contaminant proteins.

cantly, covering a range from almost double that of the wild-type enzyme down to less than 5% of the wild-type rate. The K_M values are significantly more consistent, all falling between 60% and 150% of the wild-type value. As might be expected, the thermal stability of the double mutants was consistently impaired, with all of the unfolding temperatures determined being more than 35 °C lower than the wild-type enzyme (Table 3). A selection of triple mutants were produced (L171D-L199D-I229D, L171D-L199N-I229D, L171R-L199N-I229R and L171R-L199R-I229R), however all of these mutants were found to be insoluble. Attempts to look at the insoluble mutant proteins by CD spectroscopy were thwarted by the lack of solubility, but the soluble mutants showed profiles consistent with incompletely folded protein. Representative data are shown in (Supplementary information Fig. S3).

Conclusion

The interface of NAL appears to play a critical role in functional expression. In particular, residue L171 seems key, as evidenced by the fact that of the 10 soluble mutants produced, only two carried a mutation of residue 171. Of the mutated positions, L171 interacts with its counterpart on the opposite dimer most closely (Figs. 1 and 2). Furthermore, examination of the average *B*-factors of the atoms of the mutated residues in structure 1NAL (L171: 20.4 $Å^2$, L199: 21.9 $Å^2$, I229: 40.5 $Å^2$; average for all protein atoms: 30.0 $Å^2$) suggests that L171 may be the most structurally constrained, having the lowest positional fluctuation.

The observed insolubility of interface mutants may be caused by amorphous aggregation due to exposure of hydrophobic residues upon disruption of the interface following successful folding. However, the very different behaviour of dimeric NAL enzymes to the analogous DHDPS dimer [4] and the complete absence of activity or soluble protein indicates an increased likelihood of folding itself being impaired, consistent with the CD data. For triosephosphate isomerase from *Entamoeba histolytica*, it has been recently been found that protein folding and association of monomers into an active dimer are closely coupled, and it has been suggested that the protein interface acts as a nucleation motif that directs accurate protein folding [24]. In the case of *E. coli* NAL, the failure of the majority of interface mutants to yield any soluble enzyme suggests that a similar mechanism may be operating at the dimer–dimer interface.

The paucity of soluble derivatives obtained highlights one of the potential pitfalls in efforts to engineer non-native quaternary structures. The tetrameric state appears to be a pre-requisite of functional expression. All soluble mutants remained tetrameric, but interestingly their turnover rates varied over a 40-fold range. The substrate affinity, as reflected in the K_M values, varied over only a 2-fold range. This hints at an involvement of the interface in catalysis, possibly by modulation of the dynamics of the protein as a whole.

The fact that relatively few of the mutants generated in the course of this work were even soluble sheds light on the process of evolution of interfaces. The high chance of a random mutation yielding a strongly deleterious mutation suggests that protein interfaces would be expected to evolve very slowly, although they are clearly evolutionarily more plastic than active sites for a particular enzyme [25]. This work also underlines the critical nature of protein interfaces, thus providing support for the possibility of drug development targeting interfaces rather than active sites [26]. It may be possible to design small molecules to disrupt interfaces specifically, in order to render critical homo-oligomeric proteins insoluble, and thus inactive. Furthermore, given the relatively high conservation of interface residues, targeting protein interfaces in drug discovery efforts could be expected to lead to lower rates of spontaneous development of immunity than might previously have been assumed.

Acknowledgments

S.R.A.D. would like to thank the Foundation for Science Research and Technology for postdoctoral funding (Contract UOCX0603). The authors acknowledge Renwick Dobson, Grant

Pearce and Andrew Muscroft-Taylor for helpful discussions and Jackie Healy for forthright technical assistance.

Appendix A. Supplementary data

Supplementary data associated with this article can be found, in the online version, at doi:10.1016/j.bbrc.2009.07.128.

References

[1] S. Cansu, P. Doruker, Dimerization affects collective dynamics of triosephosphate isomerase, Biochemistry 47 (2008) 1358–1368.
[2] F.G. Pearce, Catalytic by-product formation and ligand binding by ribulose bisphosphate carboxylases from different phylogenies, Biochem. J. 399 (2006) 525–534.
[3] B.R. Burgess, R.C.J. Dobson, M.F. Bailey, S.C. Atkinson, M.D.W. Griffin, G.B. Jameson, M.W. Parker, J.A. Gerrard, M.A. Perugini, Structure and evolution of a novel dimeric enzyme from a clinically important bacterial pathogen, J. Biol. Chem. 283 (2008) 27598–27603.
[4] M.D. Griffin, R.C. Dobson, F.G. Pearce, L. Antonio, A.E. Whitten, C.K. Liew, J.P. Mackay, J. Trewhella, G.B. Jameson, M.A. Perugini, J.A. Gerrard, Evolution of quaternary structure in a homotetrameric enzyme, J. Mol. Biol. 380 (2008) 691–703.
[5] S.R.A. Devenish, J.A. Gerrard, The role of quaternary structure in $(\beta/\alpha)_8$-barrel proteins: evolutionary happenstance or a higher level of structure–function relationships?, Org Biomol. Chem. 7 (2009) 833–839.
[6] S.J. Benkovic, G.G. Hammes, S. Hammes-Schiffer, Free-energy landscape of enzyme catalysis, Biochemistry 47 (2008) 3317–3321.
[7] B.B.B. Guo, S.R.A. Devenish, R.C.J. Dobson, A.C. Muscroft-Taylor, J.A. Gerrard, The C-terminal domain of *Escherichia coli* dihydrodipicolinate synthase (DHDPS) is essential for maintenance of quaternary structure and efficient catalysis, Biochem. Biophys. Res. Commun. 380 (2009) 802–806.
[8] M.C. Lawrence, J.A.R.G. Barbosa, B.J. Smith, N.E. Hall, P.A. Pilling, H.C. Ooi, S.M. Marcuccio, Structure and mechanism of a sub-family of enzymes related to *N*-acetylneuraminate lyase, J. Mol. Biol. 266 (1997) 381–399.
[9] M.E. Tanner, The enzymes of sialic acid biosynthesis, Bioorg. Chem. 33 (2005) 216–228.
[10] R. Schauer, Sialic acids: fascinating sugars in higher animals and man, Zoology 107 (2004) 49–64.
[11] E. Severi, D.W. Hood, G.H. Thomas, Sialic acid utilization by bacterial pathogens, Microbiology 153 (2007) 2817–2822.
[12] R. Louwen, A. Heikema, A. van Belkum, A. Ott, M. Gilbert, W. Ang, H.P. Endtz, M.P. Bergman, E.E. Nieuwenhuis, The sialylated lipooligosaccharide outer core in *Campylobacter jejuni* is an important determinant for epithelial cell invasion, Infect. Immun. 76 (2008) 4431–4438.
[13] U. Kragl, A. Gödde, C. Wandrey, N. Lubin, C. Augé, New synthetic applications of sialic acid aldolase, a useful catalyst for KDO synthesis. Relation between substrate conformation and enzyme stereoselectivity, J. Chem. Soc. Perkin Trans. 1 (1994) 119–124.
[14] M. von Itzstein, The war against influenza: discovery and development of sialidase inhibitors, Nat. Rev. Drug Discov. 6 (2007) 967–974.
[15] A. Dümmler, A. Lawrence, A.D. Marco, Simplified screening for the detection of soluble fusion constructs expressed in *E. coli* using a modular set of vectors, Microb. Cell Fact. 4 (2005) 34.
[16] F.W. Studier, Protein production by auto-induction in high density shaking cultures, Protein Expr. Purif. 41 (2005) 207–234.
[17] R.B. Kapust, J. Tozser, J.D. Fox, D.E. Anderson, S. Cherry, T.D. Copeland, D.S. Waugh, Tobacco etch virus protease: mechanism of autolysis and rational design of stable mutants with wild-type catalytic proficiency, Protein Eng. 14 (2001) 993–1000.
[18] U.B. Ericsson, B.M. Hallberg, G.T. DeTitta, N. Dekker, P. Nordlund, Thermofluor-based high-throughput stability optimization of proteins for structural studies, Anal. Biochem. 357 (2006) 289–298.
[19] A.C. Joerger, S. Mayer, A.R. Fersht, Mimicking natural evolution in vitro: an *N*-acetylneuraminate lyase mutant with an increased dihydrodipicolinate synthase activity, Proc. Natl. Acad. Sci. USA 100 (2003) 5694–5699.
[20] A. Cornish-Bowden, Fundamentals of Enzyme Kinetics, third ed., Portland Press, London, 2004.
[21] T. Izard, M.C. Lawrence, R.L. Malby, G.G. Lilley, P.M. Colman, The three-dimensional structure of *N*-acetylneuraminate lyase from *Escherichia coli*, Structure 2 (1994) 361–369.
[22] E. Krissinel, K. Henrick, Inference of macromolecular assemblies from crystalline state, J. Mol. Biol. 372 (2007) 774–797.
[23] G. Neshich, W. Rocchia, A.L. Mancini, et al., JavaProtein Dossier: a novel web-based data visualization tool for comprehensive analysis of protein structure, Nucleic Acids Res. 32 (2004) W595–W601.
[24] L.A. Tellez, L.M. Blancas-Mejia, E. Carrillo-Nava, G. Mendoza-Hernández, D.A. Cisneros, D.A. Fernández-Velasco, Thermal unfolding of triosephosphate isomerase from *Entamoeba histolytica*: dimer dissociation leads to extensive unfolding, Biochemistry 47 (2008) 11665–11673.
[25] W.S.J. Valdar, J.M. Thornton, Protein–protein interfaces: analysis of amino acid conservation in homodimers, Proteins: Struct. Funct. Genet. 42 (2001).
[26] J.A. Gerrard, C.A. Hutton, M.A. Perugini, Inhibiting protein–protein interactions as an emerging paradigm for drug discovery, Mini Rev. Med. Chem. 7 (2007) 151–157.